An adaptive finite element method for diffraction gratings

Gang Bao

Department of Mathematics, Michigan State University, East Lansing, MI 48824, USA.

bao@math.msu.edu

Zhiming Chen

LSEC, Institute of Computational Mathematics, Chinese Academy of Sciences, Beijing 100080, PR China.

zmchen@lsec.cc.ac.cn

Haijun Wu

Department of Mathematics, Nanjing University, Jiangsu, 210093, PR China.

hjw@nju.edu.cn

A second order finite element adaptive strategy with error control for 1-d grating problems is developed. The unbounded computational domain is truncated to a bounded one by a perfectly matched layer (PML) technique. The PML parameters such as the thickness of the layer and the medium property are determined through sharp a posteriori error estimates. The adaptive finite element method is expected to increase significantly the accuracy and efficiency of the discretization as well as to reduce the computation cost. Numerical experiments are included to illustrate the competitiveness of the proposed adaptive method.

OCIS codes: 050.0050, 200.0200.

1. Introduction

Consider 1-d grating problems both in TE polarization

$$\Delta u + k^2(x)u = 0 \tag{1}$$

and in TM polarization

$$\text{div}\left(\frac{1}{k^2(x)}\nabla u\right) + u = 0\ . \tag{2}$$

Here $u = u(x_1, x_3)$ is the second component of electric field in TE case and magnetic field in TM case, $k^2(x) = \omega^2\varepsilon(x)\mu$ is the magnitude of the wave vector. The media are assumed to be nonmagnetic and the magnetic permeability μ is constant everywhere. We assume the dielectric coefficient $\varepsilon(x) = \varepsilon(x_1, x_3)$ is periodic in x_1 direction with period $L > 0$. The dielectric coefficient $\varepsilon(x)$ may be complex. Assume that $\text{Im}\,\varepsilon(x) \geq 0$ and $\text{Re}\,\varepsilon(x) > 0$ whenever $\text{Im}\,\varepsilon(x) = 0$. It is natural to assume that ε is constant away from a region $\{(x_1, x_3) : b_2 < x_3 < b_1\}$ which includes the structure, that is, there exist constants ε_1 and ε_2 such that

$$\begin{aligned}
&\varepsilon(x_1, x_3) = \varepsilon_1 \ \text{ in } \ \Omega_1 = \{(x_1, x_3) : x_3 \geq b_1\},\\
&\varepsilon(x_1, x_3) = \varepsilon_2 \ \text{ in } \ \Omega_2 = \{(x_1, x_3) : x_3 \leq b_2\}.
\end{aligned}$$

There have been many numerical methods for modeling light diffraction by relief gratings including the differential method,[1] the s-matrix algorithm,[2] the rigorous coupled-wave approach,[3] the method of coordinate transformations,[4,5] the boundary perturbation methods,[6] the integral method,[7,8] and their extensions. Although well known for being general and efficient in the computational modeling of a broad range of scientific problems, the finite element methods (FEM) are not as popular in the diffractive optics community as some of the above mentioned methods. In our opinion, there are two main difficulties in applying the FEMs to the grating problems. The first is to truncate the domain into a bounded computational domain. The second difficulty is concerned with resolving the singularity of the solutions. Usually, the grating surface is piecewise smooth and the dielectric coefficient $\varepsilon(x)$ is discontinuous across the surface. Thus the solution of (2) has singularities which slow down the finite element convergence when using uniform mesh refinements. Even in the TE case (1), if the grating substrate is lossy, then the transmitted waves will decay exponentially, which makes uniform mesh refinements expensive. Recent studies[9,10] on finite element methods often rely on the transparent boundary condition which is represented as a nonlocal operator. In practical computation, however, the infinite series in the definition of the nonlocal operator must be truncated.

In order to overcome the above mentioned difficulties for FEMs, we have proposed recently[11] a hybrid approach which applies a perfectly matched layer (PML) technique to

truncate the unbounded domain and the modern technique of adaptive finite elements based on a posteriori error estimates to resolve the singularities.

A posteriori error estimates are computable quantities in terms of the discrete solution and data that measure the actual discrete errors without the knowledge of limit solutions. They are essential in designing algorithms for mesh modification, which equi-distribute the computational effort and optimize the computation. Ever since the pioneering work of Babuška and Rheinboldt,[12] the adaptive finite element methods based on a posteriori error estimates have become a central theme in scientific and engineering computing. One of the main advantages of adaptivity is that it provides an effective approach for modeling multiscale phenomena. Recent related studies[11,13,14,15] have shown that for appropriately designed adaptive finite element procedures, the meshes and the associated numerical complexity are quasi-optimal in the sense that the adaptive finite element procedures for any elliptic problem even with singularities converge as fast as the finite element procedures using uniform mesh refinements for elliptic problems without singularities. This makes the adaptive finite element method attractive for grating problems whose solutions often have singularities due to the discontinuity of the dielectric coefficient $\varepsilon(x)$. We refer to the related work[16,17] for solving scattering problems in general media (nonperiodic) by using adaptive methods with a posterior error estimates.

Chen and Wu[11] have recently introduced an adaptive linear (first order) finite element algorithm with PML and error control which adaptively determines the finite element meshes and the PML parameters such as the thickness of the PML region and the medium property inside the region. The goal of this paper is to develop a second order adaptive FEM. We present an adaptive second order finite element algorithm with PML based on the a posteriori error estimate. With the significantly improved accuracy, the algorithm can deal with extremely general diffractive structures and materials. The algorithm is stable, converges fast, and is easy to implement based on the existing FEM software for bounded domains. Moreover, the algorithm produces the approximate electric or magnetic field near the grating structure directly which can be used in solving optimal design problems. Finally, several challenging numerical examples are presented to illustrated the features of our adaptive FEM algorithm compared to existing methods from the literature.

2. The PML formulation

We introduce PML formulation for the 1D grating problem (1) and (2). The basic idea of the PML technique is to surround the computational domain by a nonphysical so called PML medium which can absorb without reflection outgoing waves of any frequency for any incident direction. The waves decay exponentially in magnitude into the PML medium. Thus the PML layer itself can be truncated to form a finite thickness absorbing layer with low

reflection for any angle of incidence. Another advantage of the PML technique is that it can be implemented simply. Since the work of Berenger[18] on the PML for the time dependent Maxwell equations, various constructions of PML absorbing layers have been proposed and studied in the literature. We refer to Turkel and Yefet[19] for a review of various models.

Denote by $k_j = \omega(\varepsilon_j \mu)^{1/2}$. Let $u_{\rm I} = \exp(\mathbf{i}\alpha x_1 - \mathbf{i}\beta x_3)$ be the incoming plane wave which is incident upon the grating surface from the top, where $\alpha = k_1 \sin\theta, \beta = k_1 \cos\theta$, and $-\pi/2 < \theta < \pi/2$ is the incident angle. We are interested in quasi-periodic solutions u, that is, solutions u of (1) and (2) such that $u \exp(-\mathbf{i}\alpha x_1)$ are periodic in x_1 with period $L > 0$. The radiation condition for the diffraction problem insists that u is composed of bounded outgoing plane waves in Ω_1 and Ω_2, plus the incident wave $u_{\rm I}$ in Ω_1.

Denote by $\Gamma_j = \{(x_1, x_3) : 0 < x_1 < L, x_3 = b_j\}, j = 1, 2$. We compute the solution in the bounded domain

$$\Omega = \{(x_1, x_3) : 0 < x_1 < L \text{ and } b_2 < x_3 < b_1\}.$$

We surround our computational domain Ω with two PML layers of thickness δ_1 and δ_2 in Ω_1 and Ω_2, respectively (see Fig.1). The specially designed model medium in the PML layers should be chosen so that either the wave never reaches its external boundary or the amplitude of the reflected wave is so small that it does not contaminate the solution in Ω. Let $s(x_3) = s_1(x_3) + \mathbf{i}s_2(x_3)$ be the model medium property which satisfies

$$\begin{aligned} &s_1, s_2 \in C(\mathbf{R}), \quad s_1 \geq 1, s_2 \geq 0, \\ &s(x_3) = 1 \text{ for } b_2 \leq x_3 \leq b_1. \end{aligned} \tag{3}$$

Here we remark that, in contrast to the original PML condition which takes $s_1 \equiv 1$ in the PML region, we allow a variable s_1 in order to attenuate both the outgoing and evanescent waves there. The advantage of this extension makes our method insensitive to the distance of the PML region from the structure. Introduce the PML regions

$$\begin{aligned} \Omega_1^{\rm PML} &= \{(x_1, x_3) : 0 < x_1 < L,\ b_1 < x_3 < b_1 + \delta_1\}, \\ \Omega_2^{\rm PML} &= \{(x_1, x_3) : 0 < x_1 < L,\ b_2 - \delta_2 < x_3 < b_2\}, \end{aligned}$$

and the PML differential operator

$$\mathcal{L} := \begin{cases} \frac{\partial}{\partial x_1}\left(s(x_3)\frac{\partial}{\partial x_1}\right) + \frac{\partial}{\partial x_3}\left(\frac{1}{s(x_3)}\frac{\partial}{\partial x_3}\right) \\ \qquad +k^2(x)s(x_3) \text{ for TE polarization}, \\ \frac{\partial}{\partial x_1}\left(\frac{s(x_3)}{k^2(x)}\frac{\partial}{\partial x_1}\right) + \frac{\partial}{\partial x_3}\left(\frac{1}{s(x_3)k^2(x)}\frac{\partial}{\partial x_3}\right) \\ \qquad\qquad +s(x_3) \text{ for TM polarization}. \end{cases} \tag{4}$$

As shown in Fig.1, let

$$\Gamma_1^{\rm PML} = \{(x_1, x_3) : 0 < x_1 < L, x_3 = b_1 + \delta_1\},$$
$$\Gamma_2^{\rm PML} = \{(x_1, x_3) : 0 < x_1 < L, x_3 = b_2 - \delta_2\},$$
$$D = \{(x_1, x_3) : 0 < x_1 < L, b_2 - \delta_2 < x_3 < b_1 + \delta_1\}.$$

With the PML conditions, our model problem may be reformulated as: Find $\hat{u}$ such that $\hat{u} = u_{\rm I}$ on $\Gamma_1^{\rm PML}$, $\hat{u} = 0$ on $\Gamma_2^{\rm PML}$, and

$$\mathcal{L}\hat{u} = -g \quad \text{in} \quad D \tag{5}$$

with the quasi-periodic boundary condition $\hat{u}(0, x_3) = \exp(-\mathbf{i}\alpha L)\hat{u}(L, x_3)$ for $b_2 - \delta_2 < x_3 < b_1 + \delta_1$. Here the source function

$$g = \begin{cases} -\mathcal{L}u_{\rm I} & \text{in } \Omega_1^{\rm PML}, \\ 0 & \text{elsewhere .} \end{cases}$$

Define $X(D) = \{w \in H^1(D) : w(0, x_3) = \exp(-\mathbf{i}\alpha L)w(L, x_3)\}$, and $\overset{\circ}{X}(D) = \{w \in X(D), w = 0 \text{ on } \Gamma_1^{\rm PML} \cup \Gamma_2^{\rm PML}\}$, where $H^1(\Omega)$ contains all square integrable functions whose derivatives are also square integrable on Ω. Then multiplying (5) by $\bar{\psi}$ and using integration by parts, we obtain the weak formulation of the PML model: Find $\hat{u} \in X(D)$ such that $\hat{u} = u_{\rm I}$ on $\Gamma_1^{\rm PML}$, $\hat{u} = 0$ on $\Gamma_2^{\rm PML}$, and

$$a_{_D}(\hat{u}, \psi) = \int_D g\bar{\psi}\, {\rm d}x \qquad \forall\, \psi \in \overset{\circ}{X}(D), \tag{6}$$

where the sesquilinear form $a_{_D} : X(D) \times X(D) \to \mathbf{C}$ is defined by

$$a_{_D}(\varphi, \psi) = \int_D \left(A(x)\nabla\varphi\nabla\bar{\psi} - B(x)\varphi\bar{\psi}\right)\, {\rm d}x\ . \tag{7}$$

Here

$$A(x) = \begin{pmatrix} A_{11} & 0 \\ 0 & A_{22} \end{pmatrix},$$

where

$$\begin{aligned} &A_{11} = s(x_3), \quad A_{22} = \frac{1}{s(x_3)}, \\ &B(x) = k^2(x)s(x_3) \text{ in the TE case,} \\ &A_{11} = \frac{s(x_3)}{k^2(x)}, \quad A_{22} = \frac{1}{s(x_3)k^2(x)}, \\ &B(x) = s(x_3) \text{ in the TM case.} \end{aligned} \tag{8}$$

Next we analyze the error estimates of the above problem. Let

$$\sigma_1 = \int_{b_1}^{b_1+\delta_1} s(\tau)\,\mathrm{d}\tau, \quad \sigma_2 = \int_{b_2-\delta_2}^{b_2} s(\tau)\,\mathrm{d}\tau. \tag{9}$$

Denote σ_j^R and σ_j^I the real and imaginary part of σ_j, that is, $\sigma_j = \sigma_j^R + \mathbf{i}\sigma_j^I$. Define

$$(\beta_j^n)^2 = k_j^2 - (2\pi n/L + \alpha)^2, \quad \mathrm{Im}\,\beta_j^n \geq 0.$$

In particular, if $\mathrm{Im}\,\varepsilon_2 = 0$, then

$$\beta_j^n = \beta_j^n(\alpha) = \begin{cases} \left(k_j^2 - (2\pi n/L + \alpha)^2\right)^{1/2} \\ \qquad \text{if } k_j^2 \geq (2\pi n/L + \alpha)^2, \\ \mathbf{i}\left((2\pi n/L + \alpha)^2 - k_j^2\right)^{1/2} \\ \qquad \text{if } k_j^2 < (2\pi n/L + \alpha)^2. \end{cases} \tag{10}$$

Note that $\beta_1^0 = \beta$ by definition. Assume that $k_j^2 \neq (2\pi n/L + \alpha)^2$ for all $n \in Z, j = 1, 2$. Let

$$\begin{aligned} \Delta_j^- &= \min\{\mathrm{Re}\,(\beta_j^n) : \mathrm{Re}\,(\beta_j^n) > 0\}, \\ \Delta_j^+ &= \min\{\mathrm{Im}\,(\beta_j^n) : \mathrm{Im}\,(\beta_j^n) > 0\}. \end{aligned} \tag{11}$$

Define two constants which are important in the error control and analysis:

$$M_1 = \max\left(\frac{2\Delta_1^-}{\exp(2\sigma_1^I\Delta_1^-) - 1}, \frac{2\Delta_1^+}{\exp(2\sigma_1^R\Delta_1^+) - 1}\right), \tag{12}$$

and

$$M_2 = \begin{cases} \max\left(\frac{2\Delta_2^-}{\exp(2\sigma_2^I\Delta_2^-)-1}, \frac{2\Delta_2^+}{\exp(2\sigma_2^R\Delta_2^+)-1}\right) \\ \qquad\qquad \text{if } \mathrm{Im}\,\varepsilon_2 = 0; \\ \frac{2|k_2|}{\exp(2\sigma_2^R|\mathrm{Im}\,k_2|)-1}, \qquad \text{if } \mathrm{Im}\,\varepsilon_2 > 0. \end{cases} \tag{13}$$

Under the assumptions that the original grating problem (1) (or (2)) attains a unique solution u and that the constants M_1 and M_2 are small enough, it is proved[11] that the PML variational problem (6) has a unique solution $\hat{u}$ which satisfies the following error estimate

$$\begin{aligned} &\| u - \hat{u} \|_{H^1(\Omega)} \\ &\qquad \leq CM_1 \| \hat{u} - u_{\mathrm{I}} \|_{L^2(\Gamma_1)} + CM_2 \| \hat{u} \|_{L^2(\Gamma_2)}, \end{aligned} \tag{14}$$

where $\| u - \hat{u} \|_{H^1(\Omega)}^2 = \| u - \hat{u} \|_{L^2(\Omega)}^2 + \| \nabla(u - \hat{u}) \|_{L^2(\Omega)}^2$, and C is a constant depending only on the data of the grating problem.

Now let us take a closer look at the structure of constant M_j which controls the modeling error of the PML equation towards the original 1D grating problem. Once the incoming plane wave $u_{\mathrm{I}} = \exp(\mathbf{i}\alpha x_1 - \mathbf{i}\beta x_3)$ is fixed, the numbers Δ_j^-, Δ_j^+ are fixed according to (11). Thus

the constant M_j approaches to zero exponentially as the PML parameters σ_j^R, σ_j^I tend to the infinity. From the definition (9), we know that σ_j^R, σ_j^I can be calculated by the medium property $s(x_3)$, which is usually taken as power function

$$s(x_3) = \begin{cases} 1 + \sigma_1^m \Big(\dfrac{x_3 - b_1}{\delta_1} \Big)^m & \text{if } x_3 \geq b_1 \\ 1 + \sigma_2^m \Big(\dfrac{b_2 - x_3}{\delta_2} \Big)^m & \text{if } x_3 \leq b_2 \end{cases}, \quad m \geq 1.$$

Thus

$$\sigma_j^R = \left(1 + \frac{\operatorname{Re} \sigma_j^m}{m+1} \right) \delta_j, \quad \sigma_j^I = \frac{\operatorname{Im} \sigma_j^m}{m+1} \, \delta_j. \tag{15}$$

It is obvious that to enlarge either the thickness δ_j of the PML layers or the medium parameters $\operatorname{Re} \sigma_j^m$ and $\operatorname{Im} \sigma_j^m$ will reduce the PML approximation error.

In practical applications involving the PML method, there is a compromise between a thin layer which requires a rapid variation of the artificial material property and a thick layer which requires more grid points hence more computer time and more storage. In this paper, we develop a posteriori error estimate to determine the PML parameters. Moreover, the derived a posteriori error estimate has the desirable feature of exponential decay in terms of the distance to the computational domain. This property permits the use of coarse mesh sizes away from the computational domain and hence makes the total computational cost insensitive to the thickness of the PML absorbing layer.

To conclude, we remark that the error estimate (14) is a posteriori in nature since it depends on the PML solution $\hat{u}$, which makes a posterior error control possible. See the next section for a more detailed discussion.

3. The adaptive finite element method

In this section, we introduce the finite element approximations of the PML problem (6) and establish the a posteriori error estimates. We also discuss the implementation of the adaptive algorithm.

Let $\mathcal{M}_h$ be a regular triangulation of the domain D. Recall that any triangle $T \in \mathcal{M}_h$ is considered as closed. Assume that any element T must be completely included in $\overline{\Omega_1^{\mathrm{PML}}}$, $\overline{\Omega_2^{\mathrm{PML}}}$ or $\overline{\Omega}$. To define the finite element space whose functions are quasi-periodic in x_1 direction, we also require that if $(0, z)$ is a node on the left boundary, then (L, z) is also a node on the right boundary, and vice versa. Let $V_h(D) \subset X(D)$ be the quadratic Lagrange finite element space and $\overset{\circ}{V}_h(D) = V_h(D) \bigcap \overset{\circ}{X}(D)$. Denote by $I_h : C(\bar{D}) \to V_h(D)$ the standard finite element interpolation operator.

The finite element approximation to the PML problem (6) reads as follows: Find $\hat{u}_h \in$

$V_h(D)$ such that $\hat{u}_h = I_h u_{\rm I}$ on $\Gamma_1^{\rm PML}$, $\hat{u}_h = 0$ on $\Gamma_2^{\rm PML}$ and

$$a_{_D}(\hat{u}_h, \psi_h) = \int_D g\bar{\psi}_h \,{\rm d}x \qquad \forall\, \psi_h \in \mathring{V}_h(D). \tag{16}$$

In this paper, we are interested in a posterior error estimates and the associated adaptive algorithm by assuming that the discrete problem (16) has a unique solution $\hat{u}_h \in V_h(D)$.

For any $T \in \mathcal{M}_h$, denote by h_T its diameter. Let $\mathcal{B}_h$ denote the set of all sides that do not lie on $\Gamma_j^{\rm PML}$, $j = 1, 2$. For any $e \in \mathcal{B}_h$, h_e stands for its length. For any $T \in \mathcal{M}_h$, introduce the residual

$$R_T := \mathcal{L}\hat{u}_h|_T + g|_T. \tag{17}$$

For any interior side $e \in \mathcal{B}_h$ which is the common side of T_1 and $T_2 \in \mathcal{M}_h$, define the jump residual across e

$$J_e = (A\nabla\hat{u}_h|_{T_1} - A\nabla\hat{u}_h|_{T_2}) \cdot \nu_e, \tag{18}$$

by using the convention that the unit normal vector ν_e to e points from T_2 to T_1. Denote by $\Gamma_{\rm left} = \{(x_1, x_3) : x_1 = 0, b_2 - \delta_2 < x_3 < b_1 + \delta_1\}$ and $\Gamma_{\rm right} = \{(x_1, x_3) : x_1 = L, b_2 - \delta_2 < x_3 < b_1 + \delta_1\}$. If $e = \Gamma_{\rm left} \cap \partial T$ for some element $T \in \mathcal{M}_h$ and e' is the corresponding side on $\Gamma_{\rm right}$ which is also a side of some element T', then we define the jump residual

$$\begin{aligned} J_e &= A_{11}\left[\frac{\partial}{\partial x_1}(\hat{u}_h|_T) - \exp(-{\bf i}\alpha L)\cdot\frac{\partial}{\partial x_1}(\hat{u}_h|_{T'})\right], \\ J_{e'} &= A_{11}\left[\exp({\bf i}\alpha L)\cdot\frac{\partial}{\partial x_1}(\hat{u}_h|_T) - \frac{\partial}{\partial x_1}(\hat{u}_h|_{T'})\right]. \end{aligned} \tag{19}$$

For any $T \in \mathcal{M}_h$, denote by $\eta_{_T}$ the local error estimator which is defined as follows

$$\begin{aligned} \eta_{_T} = \max_{x\in\tilde{T}}\rho(x_3)\cdot\Big[&h_T\|R_T\|_{L^2(T)} \\ &+ \Big(\frac{1}{2}\sum_{e\subset T} h_e\| \,J_e\,\|^2_{L^2(e)}\Big)^{1/2}\Big], \end{aligned} \tag{20}$$

where $\tilde{T}$ is the union of all elements having non-empty intersection with T, and

$$\rho(x_3) = \begin{cases} |s(x_3)|\exp(-R_j(x_3)) & \text{if } x \in \overline{\Omega_j^{\rm PML}}, \\ 1 & \text{if } x \in \Omega. \end{cases}$$

with $R_j(x_3)$ $(j = 1, 2)$ being defined by

$$R_1(x_3) = \min\big(\Delta_1^- \int_{b_1}^{x_3} s_2(\tau)\,{\rm d}\tau, \Delta_1^+ \int_{b_1}^{x_3} s_1(\tau)\,{\rm d}\tau\big),$$

$$R_2(x_3) = \begin{cases} \min\left(\Delta_2^- \int_{x_3}^{b_2} s_2(\tau)\,\mathrm{d}\tau, \Delta_2^+ \int_{x_3}^{b_2} s_1(\tau)\,\mathrm{d}\tau\right), \\ \qquad\qquad\qquad\qquad \text{if } \mathrm{Im}\,\varepsilon_2 = 0; \\ |\mathrm{Im}\,(k_2)| \int_{x_3}^{b_2} s_1(\tau)\,\mathrm{d}\tau, \qquad \text{if } \mathrm{Im}\,\varepsilon_2 > 0. \end{cases}$$

The following a posteriori error estimate result[11] may be used for error control in the adaptive algorithm.

$$\begin{aligned} &\| u - \hat{u}_h \|_{H^1(\Omega)} \\ &\le CM_1 \|\hat{u}_h - u_{\mathrm{I}}\|_{L^2(\Gamma_1)} + CM_2 \|\hat{u}_h\|_{L^2(\Gamma_2)} \\ &+ CM_3 \| I_h u_{\mathrm{I}} - u_{\mathrm{I}} \|_{L^2(\Gamma_1^{\mathrm{PML}})} + C\Big(\sum_{T\in\mathcal{M}_h} \eta_T^2\Big)^{\frac{1}{2}}, \end{aligned} \tag{21}$$

where $C > 0$ is a constant depending only on the minimum angle of the mesh $\mathcal{M}_h$, the thickness of the PML layers, and the grating parameters. The constants M_1 and M_2 are defined in (12) and (13), respectively. The constant M_3 is defined by

$$M_3 = \max\left(\frac{2\Delta_1^- \exp(-\Delta_1^-\sigma_1^I)}{1-\exp(-2\Delta_1^-\sigma_1^I)}, \quad \frac{2\Delta_1^+ \exp(-\Delta_1^+\sigma_1^R)}{1-\exp(-2\Delta_1^+\sigma_1^R)}\right).$$

Note that as the PML parameters σ_j^R and σ_j^I go to the infinity, the constants M_j decay exponentially. The important exponentially decay factors $\exp(-R_j(x_3))$ in the PML region Ω_j^{PML} allow us to take thicker PML layers without introducing unnecessary fine meshes away from the computational domain. Recall that thicker PML layers enhance numerical stability.

Next, we introduce the adaptive algorithm. We use the a posteriori error estimate (21) to determine the PML parameters. According to the discussion in §2, we choose the PML medium property as the power function and thus we need only to specify the thickness δ_j of the layers and the medium parameters σ_j^m (see (15)). Recall from (21) that the a posteriori error estimate consists of two parts: the PML error $\mathcal{E}_{\mathrm{PML}}$ and the finite element discretization error $\mathcal{E}_{\mathrm{FEM}}$, where

$$\mathcal{E}_{\mathrm{PML}} = M_1 \| \hat{u}_h - u_{\mathrm{I}} \|_{L^2(\Gamma_1)} + M_2 \| \hat{u}_h \|_{L^2(\Gamma_2)}, \tag{22}$$

$$\mathcal{E}_{\mathrm{FEM}} = M_3 \| \hat{u}_h - u_{\mathrm{I}} \|_{L^2(\Gamma_1^{\mathrm{PML}})} + \Big(\sum_{T\in\mathcal{M}_h} \eta_T^2\Big)^{1/2}. \tag{23}$$

$\mathcal{E}_{\mathrm{PML}}$ and $\mathcal{E}_{\mathrm{FEM}}$ should be changed accordingly in the TM case. In our implementation, we first choose δ_j and σ_j^m such that $M_j L^{1/2} \le 10^{-8}$, which makes the PML error negligible compared with the finite element discretization errors, and such that the factor $\rho(x_3)$ in (20) is not too large to guarantee numerical stability. Once the PML region and the medium property are fixed, we use the standard finite element adaptive strategy to modify the mesh according to the a posteriori error estimate (23). For any $T \in \mathcal{M}_h$, we define the local a posteriori error estimator as follows:

$$\tilde{\eta}_T = \eta_T + M_3 \| I_h u_{\mathrm{I}} - u_{\mathrm{I}} \|_{L^2(\Gamma_1^{\mathrm{PML}} \cap \partial T)}.$$

The estimators are employed to make local mesh modifications by refinement to equidistribute the approximation errors and consequently the computational effort. This naturally leads to loops of the form

$$\text{Solution} \rightarrow \text{Estimation} \rightarrow \text{Refinement}.$$

We are ready to present the adaptive algorithm developed for this work.
Algorithm. Given the tolerance $\texttt{TOL} > 0$. Let $m = 2$.

- Choose δ_1, δ_2, and σ_j^m such that $M_j L^{1/2} \leq 10^{-8}$ $(j = 1, 2)$ and $\rho(b_1+\delta_1/2), \rho(b_2-\delta_2/2) < 1.5$;
- Generate an initial mesh $\mathcal{M}_h$ over D;
- While $\mathcal{E}_{\text{FEM}} > \texttt{TOL}$ do
  - Choose a set of elements $\widehat{\mathcal{M}}_h \subset \mathcal{M}_h$ such that

$$\left(\sum_{T \in \widehat{\mathcal{M}}_h} \tilde{\eta}_T^2 \right)^{1/2} > 0.7 \left(\sum_{T \in \mathcal{M}_h} \tilde{\eta}_T^2 \right)^{1/2},$$

    then refine the elements in $\widehat{\mathcal{M}}_h$. Denote the new mesh by $\mathcal{M}_h$ also.
  - solve the discrete problem (16) on $\mathcal{M}_h$
  - compute error estimators on $\mathcal{M}_h$

  end while

4. Numerical examples

We report several challenging examples from the literature to demonstrate the competitiveness of our algorithm. In all of the experiments, let λ and n denote the wavelength of the incident wave and refractive index, respectively.

Example 1. Lamellar grating.[20, 21] The grating is shown in Fig. 2 with the incident angle $\theta = \pi/6$ and wavelength $\lambda = 1\mu$m. This is a standard test problem used by many researchers. According to [20, Granet], the computed efficiency of the reflected zeroth order is 0.7342789 for TE polarization and 0.8484781 for TM polarization. It appears from Granet's results that the efficiency does converge to the value 0.7342789 for TE while the convergence to the value 0.8484781 for TM is not clear. As shown in Table 1, the value of our computed zeroth order efficiency for TE after 26 adaptive refinements is 0.7342790 which agrees well with the value of Granet. In the TM case, our result after 21 adaptive refinements is 0.8484782 which

is close to that of Granet. It seems that our result 0.8484815 after 28 adaptive refinements is better. We also present in the table the results computed by using uniform mesh refinements. It can be seen that under the same DoFs (degree of freedoms of the finite element equation), the result obtained by using the adaptive mesh is more accurate than the one obtained by using the uniform mesh, while the computation time is longer because the adaptive algorithm involves additional operations such as a posteriori error estimates. In the TE case, the best result can be achieved by using a uniform mesh on our computer is 0.7342874 for a CPU time of 337.6s (on an Intel 2.6Hz PC). It only needed 89.7s to achieved a better result by using the adaptive algorithm. In the TM case, the best result is 0.8484319 by using a uniform mesh for a CPU of 288.5s. Only 44.2s was needed to achieved a slightly better result by using the adaptive algorithm.

Example 2. Multilayer waveguide grating.[22] The profile of the grating is plotted in Fig. 3. The incident angle is $\theta = 0$. Fig. 4 plots the zeroth order reflected efficiency as a function of wavelength. The result agrees well with that of [22, Wang and Magnusson].

Example 3. Cylindrical rod grating.[23] Consider a periodic array of cylindrical, metallic rods in TM polarization. The groove spacing is 1μm, the radius r of the rods is 0.5μm, and their refractive index is $1.3 + 7.6\mathbf{i}$. They are placed in the vacuum and shined under 30° incidence angle by a 0.6328μm wavelength laser. Fig. 5 plots the total efficiency as a function of DoFs. The figure confirms that the adaptive algorithm converges fast. The mesh and the surface plots of the real part of the associated solution after 44 adaptive refinements are shown in Fig. 6.

Example 4. Rectangular rods grating.[23] We analyze numerically the effect recently announced[24] which has attracted a great deal of interest in the community. Consider a rectangular rod grating in TM polarization. The rods are made with silver. The groove spacing is 0.9μm, the groove height is 0.2μm, and the groove width is 0.02μm with normal incidence. The rods lie on a glass substrate with refractive index 1.44. Fig. 8 shows the zeroth order transmitted intensity as a function of the wavelength. Our result is slightly different from the result of [23, Popov and Neviére] perhaps caused by the different data of refractive indices for sliver. The groove width of 0.02μm corresponds to a filling ratio of 0.978, the same as for the two-dimensional grating consisting of small cylindrical holes in a metallic sheet.[24] Although our analysis relies on an one dimensional model described in Ref. 26, the expected extraordinary transmission through subwavelength hole arrays is found as well as the expected peaks due to surface plasma. Fig. 9 presents the mesh and the surface plots of the real part of the associated solution after 14 adaptive iterations in the case of $\lambda = 0.984$.

Example 5. Covered echelle grating. It is well known that below 160nm the reflectivity and thus the efficiency of aluminum gratings degrades because of the edge absorption of the oxide layer that naturally forms upon a surface exposed to the air. To eliminate the

absorption, sometimes magnesium fluoride may be deposited onto the surface immediately after the grating replication to prevent the aluminum from oxidizing.[7] The current example deals with an aluminium echelle with 316 grooves/mm, working blaze angle 63.4° and apex angle 90°. The grating exhibits a high efficiency at the -47th order in TM polarization at the wavelength $\lambda = 120$ nm. A protecting MgF_2 layer of thickness 25nm is applied. Fig. 10 gives the -47^{th} order efficiency as a function of DoFs. It is easily seen that the algorithm converges. The mesh and the surface plots of the real part of the associated solution near the apex after 14 adaptive iterations are shown in Fig 11. Finally, we present the total efficiency and the -47^{th} order efficiency plots as functions of wavelength in Fig 12.

5. Conclusion

We have developed a second order finite element adaptive algorithm along with a PML technique. The algorithm is general, effective, systematic, and easy to implement based on the existing FEM software for bounded domains. It is currently being extended to the three dimensional case (crossed gratings).

Acknowledgements

The research of the first author was supported in part by the NSF grant DMS 01-04001, the ONR grant N000140210365, and the NSF of China grant 10428105, and a special research grant from the KLA Tencor Foundation. This second author was supported in part by the NSF of China grant 10025102 and by China MOST under the grant G1999032802. The research of the third author was supported partially by the NSF of China grant 10401016.

References

1. M. Neviére, G. Cerutti-Maori, and M. Cadilhac, "Sur une nouvelle méthode de résolution du probléme de la diffraction d'une onde plane par un réseau infiniment conducteur," Opt. Commun. **3,** 48–52 (1971).
2. L. Li, "Formulation and comparison of two recursive matrix algorithms for modeling layered diffraction gratings," J. Opt. Soc. Am. A **13,** 1024-1035 (1996).
3. M. G. Moharam and T. K. Gaylord, "Diffraction analysis of dielectric surface-relief gratings," J. Opt. Soc. Am. **72,** 1385–1392 (1982).
4. J. Chandezon, M. T. Dupuis, G. Cornet, and D. Maystre, "Multicoated gratings: a differential formalism applicable in the entire optical region," J. Opt. Soc. Am. **72,** 839–846(1982).
5. L. Li, "Oblique-coordinate-system-based Chandezon method for modeling one-dimensionally periodic, multilayer, inhomogeneous, anisotropic gratings," J. Opt. Soc. Am. A **16,** 2521–2531 (1999).

6. O.P. Bruno and F. Reitich, "Numerical solution of diffraction problems: A method of variation of boundaries," J. Opt. Soc. Am. A **10,** 1168–1175(1993).
7. E. Popov, B. Bozhkov, D. Maystre, and J. Hoose, "Integral method for echelles covered with lossless or absorbing thin dielectric layers," Applied optics **38,** 47–55 (1999).
8. D.W. Prather, M.S. Mirotznik, and J.N. Mait, "Boundary integral methods applied to the analysis of diffractive optical elements," J. Opt. Soc. Am. A, **14,** 34–43 (1997).
9. G. Bao, D. C. Dobson, and J. A. Cox, "Mathematical studies in rigorous grating theory," J. Opt. Soc. Am. A **12,** 1029–1042 (1995).
10. G. Bao, L. Cowsar, and W. Masters, ed. "Mathematical Modeling in Optical Sciences", SIAM Frontiers in Appl. Math, SIAM, Philadelphia, 2001.
11. Z. Chen and H. Wu, "An adaptive finite element method with perfectly matched absorbing layers for the wave scattering by periodic structures," SIAM J. Numer. Anal. **41,** 799–826 (2003).
12. I. Babuška and C. Rheinboldt, "Error estimates for adaptive finite element computations," SIAM J. Numer. Anal. **15,** 736–754 (1978).
13. P. Morin, R.H. Nochetto and K.G. Siebert, "Data oscillation and convergence of adaptive FEM," SIAM J. Numer. Anal. **38,** 466–488 (2000).
14. Z. Chen and S. Dai, "On the efficiency of adaptive finite element methods for elliptic problems with discontinuous coefficients," SIAM Journal on Scientific Computing **24,** 443–462 (2002).
15. R. Verfürth, *A Review of A Posteriori Error Estimation and adaptive Mesh Refinement Techniques,* (Teubner, 1996).
16. P. Monk, "A posteriori error indicators for Maxwell's equations," J. Comput. Appl. Math. **100,** 173–190 (1998).
17. P. Monk and E. Süli, "The adaptive computation of far-field patterns by a posteriori error estimation of linear functionals," SIAM J. Numer. Anal. **36,** 251–274 (1998).
18. J.-P. Berenger, "A perfectly matched layer for the absorption of electromagnetic waves," J. Comput. Physics **114,** 185–200 (1994).
19. E. Turkel and A. Yefet, "Absorbing PML boundary layers for wave-like equations," Appl. Numer. Math **27,** 533–557 (1998).
20. G. Granet, "Reformulation of the lamellar grating problem through the concept of adaptive spatial resolution," J. Opt. Soc. Am. A **16,** 2510–2516 (1999).
21. P. Lalanne and J.-P. Hugonin, "Numerical performance of finite-difference modal methods for the electromagnetic analysis of one-dimensional lamellar gratings," J. Opt. Soc. Am. A **17,** 1033–1042 (2000).
22. S.S. Wang and R. Magnusson, "Multilayer waveguide-grating filters," Applied optics **34**, 2414–2420 (1995).

23. E. Popov and M. Neviére, "Grating theory: new equations in Fourier space leading to fast converging results for TM polarization," J. Opt. Soc. Am. A **17,** 1773–1784 (2000).
24. T. W. Ebbesen, H. J. Lezec, H. F. Ghaemi, T. Thio, P. A. Wolff, "Extraordinary optical transmission through subwavelength hole arrays," Nature **391,** 667–669 (1998).

Adaptive mesh				Uniform mesh			
k	DoFs	R_{-1}	Time (s)	k	DoFs	R_{-1}	Time (s)
TE				TE			
0	634	0.8296302	2.2	0	634	0.8296302	2.2
4	974	0.7532184	9.6	1	2580	0.7539385	2.8
9	2886	0.7358690	20.3	2	10312	0.7361900	5.0
12	6002	0.7346205	29.2	3	41616	0.7344127	15.6
19	40859	0.7342833	89.7	4	165664	0.7342874	337.6
22	90263	0.7342805	181.2	5	Out of	memory	
24	153161	0.7342795	479.0				
26	254493	0.7342790	1711.6				
TM				TM			
0	634	0.8257977	2.4	0	634	0.8257977	2.2
6	1666	0.8447566	13.9	1	2580	0.8440450	2.6
10	3938	0.8481898	23.5	2	10312	0.8478312	4.7
13	7580	0.8483288	33.8	3	41616	0.8483253	15.7
15	12217	0.8484497	44.2	4	165664	0.8484319	288.5
21	44695	0.8484782	113.6	5	Out of	memory	
27	162453	0.8484814	649.8				
28	201205	0.8484815	1007.0				

Table 1. Zeroth order efficiencies and computation time for Example 1. k : number of refinements; DoFs: degree of freedoms.

List of Figure Captions

Fig. 1. Geometry for the PML problem.

Fig. 2. Problem geometry for Example 1.

Fig. 3. Problem geometry for Example 2. The period is 0.3μm. The thicknesses of the layers corresponding to n_2, n_3, and n_4 are $0.188, 0.063$, and 0.068μm, respectively.

Fig. 4. TE spectral response of a triple-layer waveguide-grating filter of Example 2.

Fig. 5. Grating efficiency of Example 3 as a function of DoFs.

Fig. 6. The mesh and the surface plots of the real part of the associated solution of Example 3 after 44 adaptive iterations. TM case.

Fig. 7. Problem geometry for Example 4. The period is 0.9μm, the groove height is 0.2μm, and the groove width is 0.02μm. The sliver rods lie on a glass substrate with refractive index 1.44.

Fig. 8. Zeroth order transmitted efficiency of a silver rectangular rod grating lying on a glass substrate, as a function of the wavelength. The extraordinary transmission through sub-wavelength hole arrays is found when the wavelength is near 0.984.

Fig. 9. The mesh and the surface plots of the real part of the associated solution of Example 4 after 14 adaptive iterations. $\lambda = 0.984$. TM case.

Fig. 10. The -47^{th} order efficiency as a function of DoFs. Echelle grating: 316 gr/mm, blaze angle 63.4°. Coating:MgF_2, thickness 25nm. TM. $\lambda = 120$ nm.

Fig. 11. The mesh and the surface plots of the real part of the associated solution of Example 5 near the apex after 14 adaptive iterations. TM case.

Fig. 12. Total efficiency and -47^{th} order efficiency versus the wavelength. Echelle grating: 316 gr/mm, blaze angle 63.4°. Coating:MgF_2, thickness 25nm. TM. Mode: -47th order.

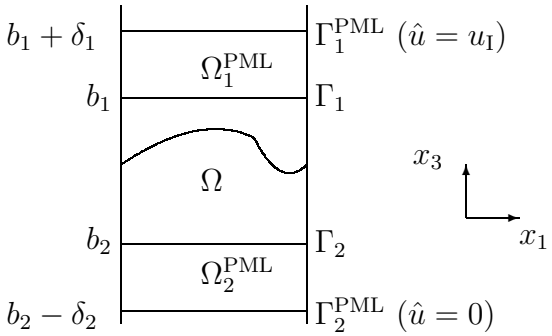

Fig. 1. Geometry for the PML problem.

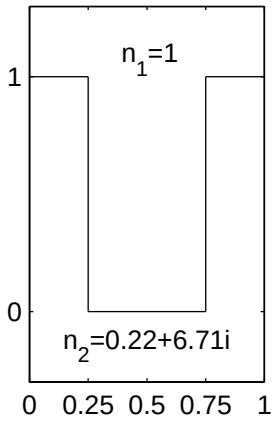

Fig. 2. Problem geometry for Example 1.

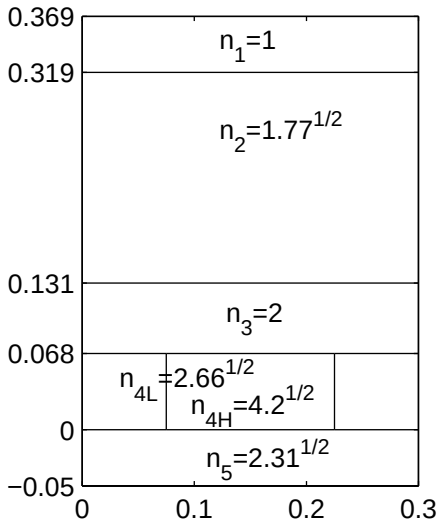

Fig. 3. Problem geometry for Example 2: The period is 0.3μm. The thicknesses of the layers corresponding to n_2, n_3, and n_4 are $0.188, 0.063$, and 0.068μm, respectively.

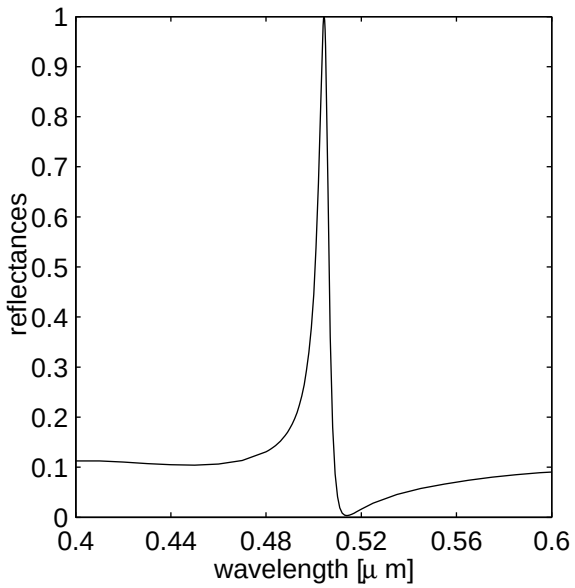

Fig. 4. TE spectral response of a triple-layer waveguide-grating filter of Example 2.

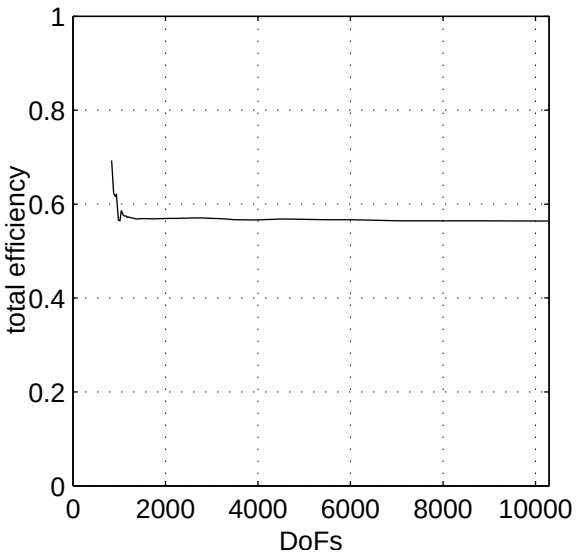

Fig. 5. Grating efficiency of Example 3 as a function of DoFs.

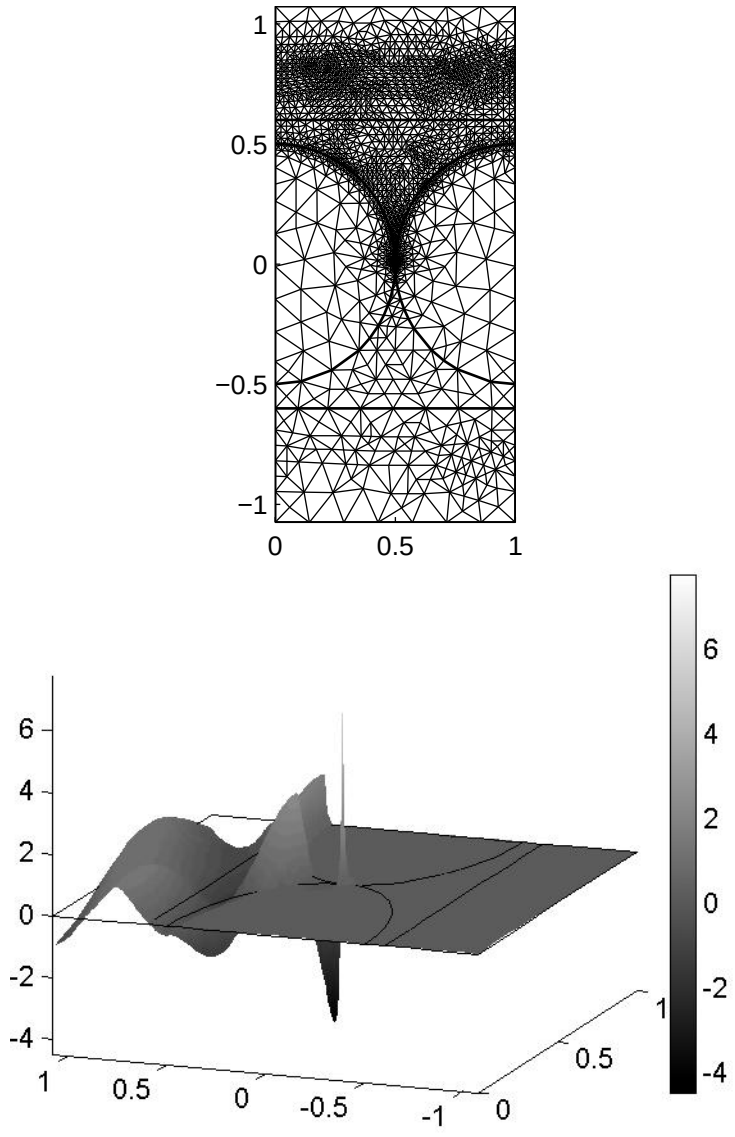

Fig. 6. The mesh and the surface plots of the real part of the associated solution of Example 3 after 44 adaptive iterations in the TM case.

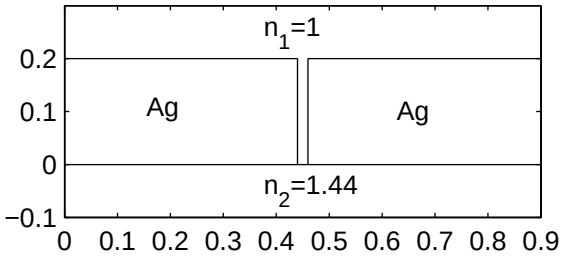

Fig. 7. Problem geometry for Example 4: The period is 0.9μm. The groove height is 0.2μm, and the groove width is 0.02μm. The sliver rods lie on a glass substrate with refractive index 1.44.

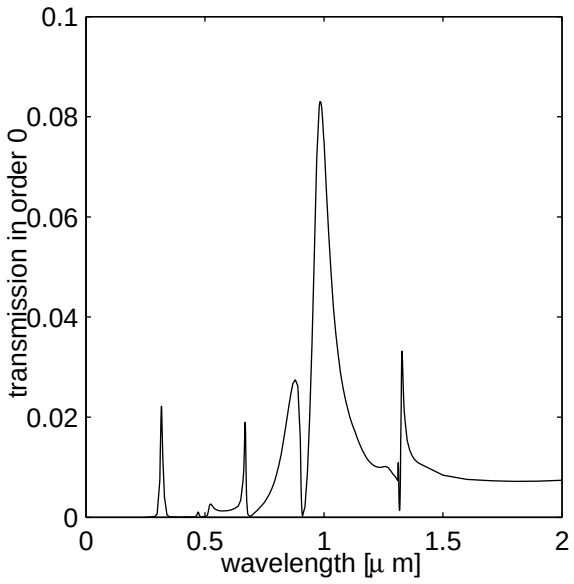

Fig. 8. Zeroth order transmitted efficiency of a silver rectangular rod grating lying on a glass substrate, as a function of the wavelength. The extraordinary transmission through sub-wavelength hole arrays is found when the wavelength is near 0.984.

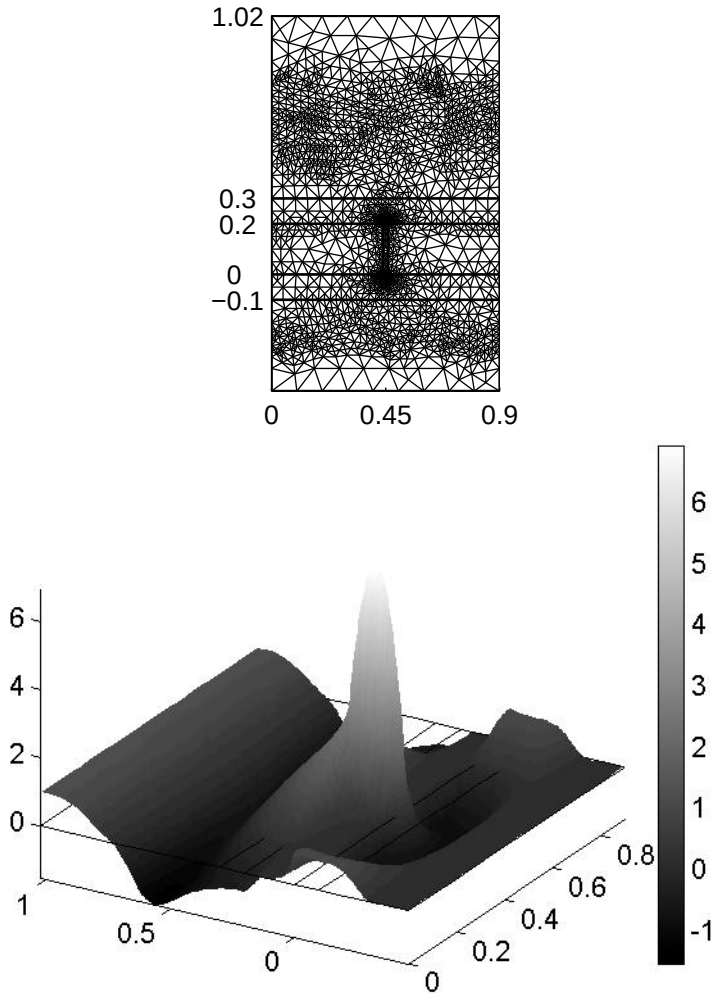

Fig. 9. The mesh and the surface plots of the real part of the associated solution of Example 4 after 14 adaptive iterations. $\lambda = 0.984$ in the TM case.

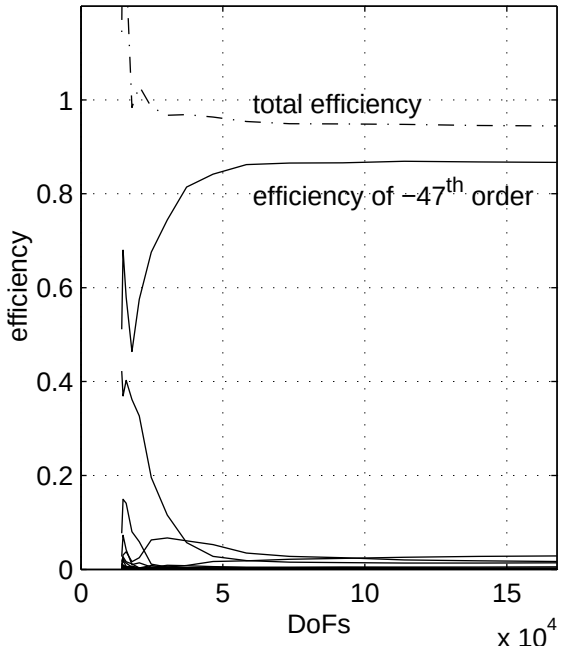

Fig. 10. The -47^{th} order efficiency as a function of DoFs in the TM case. Echelle grating: 316 gr/mm, blaze angle 63.4°, the thickness for MgF_2 coating 25nm, and $\lambda = 120$ nm

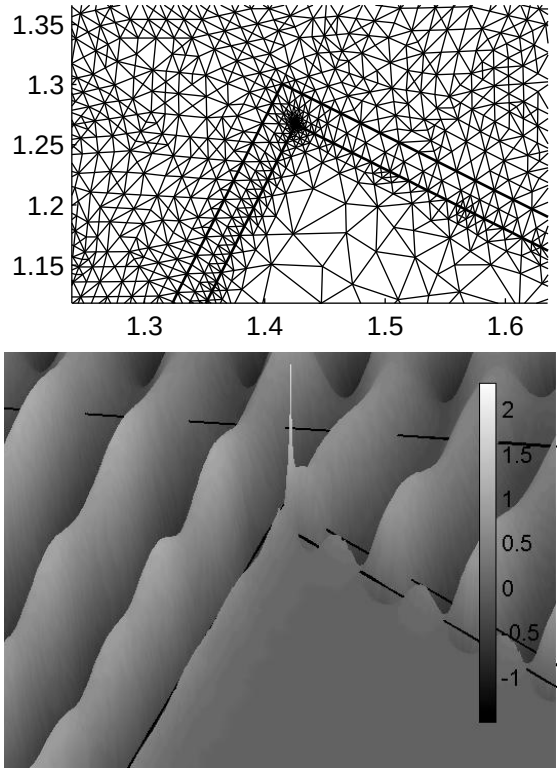

Fig. 11. The mesh and the surface plots of the real part of the associated solution of Example 5 near the apex after 14 adaptive iterations in the TM case.

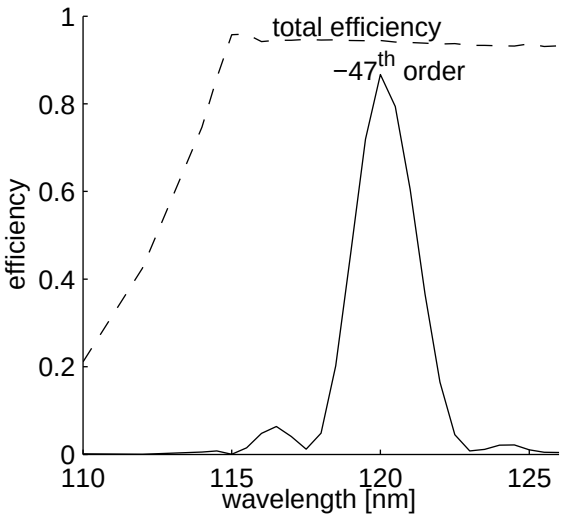

Fig. 12. Total efficiency and -47^{th} order efficiency as functions of the wavelength. Echelle grating: 316 gr/mm, blaze angle 63.4°. Coating:MgF_2, thickness 25nm. TM. Mode: -47th order.